CONFERENCE PRE-PRINT

NOVEL EFFECTS OF EDGE-LOCALISED RMPS AND PLASMA DENSITY ON THE L-H TRANSITIONS AND TRANSPORT

E. KIM Coventry University Coventry, United Kingdom Seoul National University Seoul, Republic of Korea Email: ejk92122@gmail.com

S.J. HAN and J.-K. PARK Seoul National University Seoul, Republic of Korea

M.J. CHOI, W.H. Ko, J.W. JUHN, J.H. SEO, H.S. KIM, and KSTAR TEAM Korea Institute of Fusion Energy Daejeon, Republic of Korea

S.M. YANG Princeton Plasma Physics Laboratory Princeton, United States of America

Abstract

KSTAR studies of L–H/H–L access using the upgraded low single-null (LSN) tungsten divertor and the carbon upper single-null (USN) divertor are reported. In the tungsten LSN configuration, the L–H transition is temporally more variable than in the earlier carbon LSN case, exhibiting repeated L–H/H–L cycling. In line with prior studies, the power threshold is density- and configuration-dependent; the present analysis maps this dependence for KSTAR and identifies the density at which the threshold is minimized. Power-ramping history acts as a hidden variable—different schemes (step versus linear, differing ramp rates) introduce significant scatter in the L–H threshold, consistent with theoretical expectations. Magnetic fluctuations are ubiquitous, but their impact depends on density and configuration, shifting between broadband turbulence and quasi-coherent modes. Applying n=1 edge resonant magnetic perturbations (ERMPs) produce multi-faceted effects, including L–H avoidance, H–L triggering, transient ELM suppression, spectral restructuring, and hysteresis. Pre-emptive ERMPs (applied in L-mode) can briefly raise performance but lead to a shorter-lived, more unstable H-mode, underscoring the need to control ramp history and optimize ERMP parameters to achieve sustained high performance.

1. INTRODUCTION

Understanding the low-to-high (L–H) confinement transition is essential for achieving H-mode access in ITER and advanced scenarios. Despite more than 40 years of research, key questions remain—especially the roles of hidden variables and magnetic fluctuations [1–5]. This paper reports results from 2024 KSTAR experiments using the newly upgraded tungsten lower single null (LSN) divertor and edge-localized magnetic perturbations (ERMPs) [3,5] in the upper carbon single null (USN) divertor. Here, ERMPs preferentially affect edge-localized modes (ELMs) in the edge plasma while preserving high core confinement [6], in contrast to conventional RMPs, which can trigger instabilities such as locked modes and degrade core performance.

Experiments were conducted at toroidal magnetic field B_T =1.9 T and plasma current Ip=0.6 MA over a density range $n_e = 1.5 - 3.5 \times 10^{19}$ m⁻³. Neutral beam injection (NBI) provided the primary heating. Density feedback control maintained constant L-mode density, and brief NBI blips (every 1 s) were used for charge-exchange spectroscopy (CES) measurements of ion temperature and toroidal rotation. In the LSN tungsten divertor the magnetic drift is favourable, whereas in the USN carbon divertor it is unfavourable. For USN discharges, we applied n=1 optimised ERMPs.

The key findings are summarised as follows:

- Multiple L-H and H-L transitions in the tungsten LSN divertor: L-H transitions are temporally more variable, with repeated L-H and H-L transitions, compared with those observed in the previous carbon LSN divertor (Sec. 2).
- **Density and USN/LSN dependence of the power threshold:** Identification of a rollover density at which the power threshold reaches a minimum value (Sec. 2).
- **Power ramping scenarios:** Different ramping schemes introduce scatter in the L–H transition power threshold due to transient effects, which act as hidden variables, consistent with theoretical predictions [4] (Sec. 2).
- **Prevalent magnetic fluctuations:** Magnetic fluctuations are ubiquitous across all densities but exhibit different characteristics and contributions to transport depending on plasma density (Secs. 3–5).
- **ERMP effects in USN:** In USN, ERMPs delay the L-H transition, suppress ELMs, and coherent modes, trigger H-L transitions, and modify the spectrogram of magnetic fluctuations (Sec. 5).
- **Hysteresis induced by ERMPs:** When applied briefly in L-mode, ERMPs lead to a more unstable H-mode compared with discharges without ERMPs. Thus, ERMPs can induce hysteresis, destabilize the plasma, and increase the L-H power threshold (Sec. 5).

Details are presented in Sections 2–5, with conclusions in Section 6.

2. L-H TRANSITION POWER THRESHOLD P_{net}

We use the following discharges

USN: #35632, #35633, #35634, #35638, #35640, #35641, #35643, #37404, #37405

LSN: #35645, #35646, #35637, #37407

and calculate the L-H and H-L transition power threshold as follows

$$P_{net} = P_{ohm} + P_{NBI} - \frac{dW_{mhd}}{dt} - P_{rad} \tag{1}$$

Here, P_{ohm} , P_{NBI} , W_{mhd} , and P_{rad} , respectively, represent the Ohmic power, NBI power, plasma energy, and radiation loss power. Ohmic power P_{ohm} was obtained by $P_{ohm} \approx I_P \times V_{loop}$ where V_{loop} is the average loop voltage over LV01, LV12, LV23, LV34, and LV45.

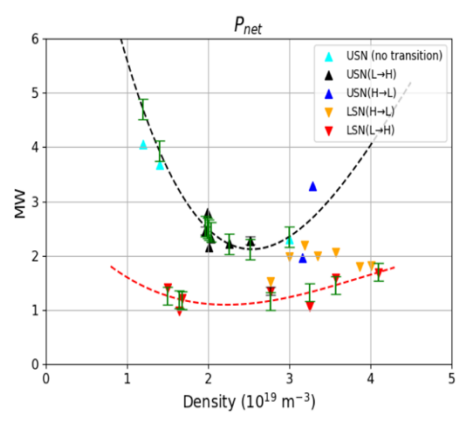


Fig. 1 P_{net} against density for multiple L-H and H-L transitions.

Figure 1 plots P_{net} versus instantaneous density at the L-H transition, combining data from multiple L–H and H–L transitions. Upper triangles denote USN discharges (black: L–H threshold; blue: H–L threshold), and lower triangles denote LSN discharges (red: L–H; yellow: H–L). Three shots that did not access H-mode are shown in sky blue. The black and red dashed curves are cubic fits to the L–H threshold for USN and LSN, respectively. For the three non-transitioning shots, P_{net} values slightly above the maximum P_{net} achieved in L-mode were assigned for fitting. Green error bars at each point indicate the fit uncertainty.

 P_{net} is clearly larger in USN than in LSN—typically by a factor of two or more. The rollover density at which P_{net} is minimised is $n_e \sim 2.5 \times 10^{19} \text{ m}^{-3}$. Around $n_e \sim 2 \times 10^{19} \text{ m}^{-3}$, four USN data points (black upper triangles; shots #35638, #35640, #35641, #35643) were

obtained under NBI power-ramping scenarios that included stepwise increases and linear ramps at 0.30 and 0.45 MW/sec. The highest threshold occurred with a large step increase (#35638), whereas the lowest threshold was observed for the slow linear ramp (0.30 MW/sec) consistent with reduced transient drive. Taken together, the data indicate that the power-ramping rate introduces uncertainty in the power threshold, functioning as a hidden variable, and confirm the theoretical prediction [4]. The power threshold is higher in USN than in LSN.

Furthermore, around $n_e \sim 2 \times 10^{19}$ m⁻³, we examine a 'pre-emptive ERMP' case (#37404), in which ERMPs are applied during L-mode ahead of the anticipated L–H transition and are switched off before the transition (see Sec. 5). This discharge shows a slightly larger P_{net} than the conventional ERMP case #35641.

3. COMPARISON OF USN AND LSN DISCHARGES AT L-MODE DENSITY $n_e \sim 1.5, 2 \ x 10^{19} \ m^{-3}$

Figure 2 presents the time histories of principal plasma parameters for LSN #35645 (red) and USN #35641 (black), each operated with L-mode density-feedback control at $n_e \sim 2 \times 10^{19}$ m⁻³. The L–H transition times are marked by vertical lines (red and black, respectively). To secure L–H access in USN, a higher NBI power was applied in shot #35641.

For #35645 (LSN), the L–H transition occurs before the linear power ramp. With increasing heating power, repeated L–H/H–L transitions are observed. Such cycling is not seen in the USN case. In the USN discharges, however, small ELMs appear soon after the L–H transition and evolve into larger ELMs (see the third panel). Overall, the plasma energy W_{mhd} ,

normalized beta β_n , ion temperature T_i , and toroidal velocity V_T are higher in USN in the H-mode (due to higher NBI power).

Fig. 2 Time traces of Ip, Pnbi, $D\alpha$, Wmhd, β_n , n_e , Ti, and V_T from the top to bottom. Red and black are for #35645 and #35641, respectively. Solid lines and dotted lines in the time traces of Ti and V_T are for the core and edge plasmas. L-H transition times are marked by the vertical lines at t=5.23 secs, t=4.1 secs for #35641 and #35645, respectively.

3.1 LSN plasmas

In the LSN, W_{mhd} , β_n , T_i , V_T , and n_e all increase at the L-H transition and remain well correlated throughout H-mode. Notably, they also correlate with broadband electron-temperature fluctuations (T_e) fluctuation as seen in the spectrograms of Fig. 4 but show weak correlation with magnetic or density fluctuations. In fact, broadband magnetic and density fluctuations are suppressed at the L-H transition, although coherent magnetic fluctuations near 10 and 20 kHz persist into H-mode. These observations suggest $T_e - n_e$ decoupling at low density and suppression of random fluctuations by E_r shear in H-mode.

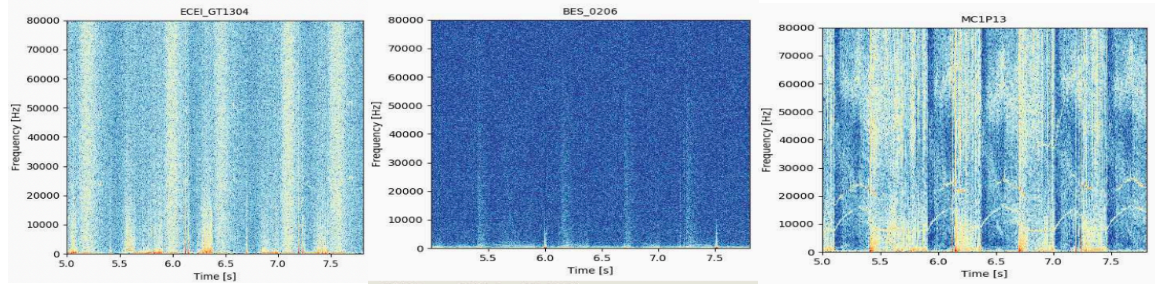


Fig 3. Spectrograms of electron temperature, density and magnetic fluctuations for #35645. Note phase shift between MC (BES) and ECEI. L-H transition at t=4.1 secs at density 1.5×10^{19} m³.

More specifically, across the L–H transition, strong Er shear suppresses the broadband magnetic and density fluctuations characteristic of L-mode—likely arising from drift-Alfvén/ballooning and microtearing mode (MTM) [7] at the edge. In the quieter H-mode background, however, discrete electromagnetic modes become prominent: coherent magnetic fluctuations near 10 and 20 kHz persist, with frequencies that rise with heating power and scale approximately as $T_e^{0.5}$ or $n_e^{0.5}$. This scaling is reminiscent of BAEs¹—finite- β , sound-speed–scaled gap modes destabilized by fast-ion pressure gradients [8, 9]—and may also overlap with pedestal-top MTM signatures [7]. At the same time, broadband electron-temperature fluctuations appear in H-mode but are not coincident with the magnetic spectrum, suggesting a different origin. Their persistence is consistent with trapped-electron-mode (TEM) or ETG-like turbulence [10], which is less susceptible to Er shear and primarily drives electron heat transport with weak magnetic signatures. In addition, downward-chirping modes starting near 80 kHz are observed in H-mode together with the 10–20 kHz line. These chirps are characteristic of energetic-particle—driven Alfvénic

¹ Because finite-β and geodesic curvature couple the Alfvén and ion-acoustic branches (forming the BAE gap), BAEs are weakly compressible. That, plus convective modulation near the mode/island or E×B flows, can yield a small but coherent Te fluctuation at the BAE frequency.

modes (TAE/RSAE/EPM) and likely reflect nonlinear EP redistribution in the improved-confinement regime. Taken together, these observations indicate that the L–H transition suppresses broadband turbulence but enables the coexistence of coherent low-frequency electromagnetic modes, residual electron-branch turbulence, and EP-driven Alfvénic activity in H-mode.

Furthermore, at the L–H transition, a strong pedestal forms in the V_T profile for R > 2.2 m with a steep edge gradient, whereas no comparable edge transport barrier appears in T_i . Notably, the onset of the L–H transition is marked by a sudden increase in V_T across the core plasma up to $R \sim 2.2$ m. During the repeated L–H/H–L transitions, the overall magnitude of V_T varies in time, but its radial shear in the core remains nearly unchanged. This relatively flat radial V_T suggests the efficient momentum transport at low density.

3.2 USN plasmas

As in the LSN case (#35645), W_{mhd} , β_n , T_i , and n_e are correlated in H-mode; low-frequency (<80 kHz) magnetic fluctuations appear before the L-H transition and are then suppressed in H-mode. Quasi-coherent modes near 15 and 30 kHz persist through H-mode, appearing between frequent ELM bursts. The key difference is that these coherent electromagnetic features correlate more with n_e fluctuations but not with T_e fluctuations. suggesting a shift in the observed coupling toward pressure-coupled electromagnetic responses (e.g., ballooning-like branches or dissipative TEM). This may reflect differing edge conditions between USN and LSN, weaker Er shear in the USN H-mode compared with the LSN H-mode of #35645 (not shown), and higher heating power in USN. A more detailed study is warranted to identify the dominant cause.

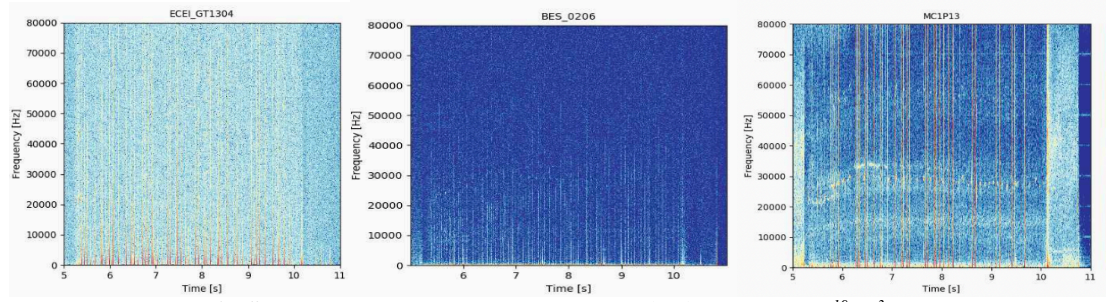


Fig 4. Spectrograms for #35641. L-H transition at t=5.23 secs at the density 2.04×10^{19} m⁻³

4. L-H TRANSITIONS AT HIGHER DENSITY IN LSN

In Section 3, we compared USN and LSN plasmas at low density. We now examine higher-density LSN plasmas.

4.1 Spectra

Figure 5 shows spectra of electron-temperature, density, and magnetic fluctuations for the highest-density case n_e =3.57 x10¹⁹ m⁻³. In contrast to Figs. 3–4, the L-mode exhibits discrete magnetic peaks near 10 and 20 kHz rather than a broadband spectrum, whereas broadband activity (including low-frequency power at 0–5 kHz) appears across the L–H transition and in H-mode. At approximately the same time, broadband fluctuations emerge in the T_e and T_e spectra. The subsequent H–L transition is marked by the disappearance of these broadband oscillations. To interpret this behaviour, note that in NBI-heated plasmas at intermediate-to-high density, strong fast-ion drive with only moderate damping can favour Alfvénic eigenmodes (TAE/BAE/GAE), which appear as narrow, coherent lines on Mirnov coils and, depending on localization and diagnostic sensitivity, may also imprint on T_e .

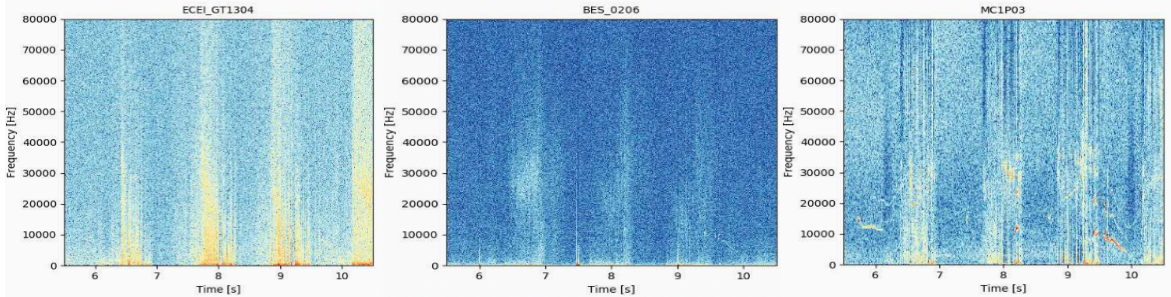


Fig 5. High-density plasmas #35647: from the left to right, electron temperature, density, and magnetic fluctuation spectrograms. The first L-H transition at t=6.4 secs at $n_e=3.57\times10^{19}$ m⁻³.

To investigate this further, Fig 6 shows the evolution of the line-averaged density (top) and the toroidal mode

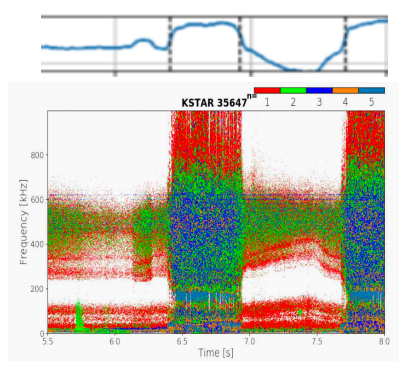


Fig 6. Toroidal n mode spectrum for $35647 (n_e = 3.57 \times 10^{19} \text{ m}^{-3})$

spectrum of magnetic fluctuations. In L-mode, the n=1 branch exhibits $f \propto 1/\sqrt{n_e}$, i.e. the frequency decreases as density rises, consistent with Alfvénic scaling [8]. Using $B_T=1.9$ T, and $n_e \simeq (2-3.5) \times 10^{19} \mathrm{m}^{-3}$ (deuterium), the Alfven speed $v_A=\frac{B}{\mu_0 n_e m_i} \sim (6.6-5) \times 10^6$ m/s. The TAE frequency then follows $f_{TAE}=\frac{v_A}{4\pi q_R} \approx (30-72)$ kHz assuming $q \approx 4-7$, and R=1.8 m. A higher band frequency $f_{GAE} \sim \frac{v_A}{2\pi R} \sim 440-580$ kHz seems consistent with GAE [11]. In H-mode, the magnetic spectrum becomes broad with overlapping toroidal mode n, suggesting coexistence of Alfvénic activity and additional branches (e.g. MTM/KBM). Concurrently, the toroidal rotation shear drops markedly in the H-mode; this can be due to increased momentum transport (flattening $V_T(r)$).

Fig 7. (Left) Magnetic spectrum; (Right) T_e fluctuation spectrum for 35646 ($n_e = 3.2 \times 10^{19}~m^{-3}$)

Another case with coherent fluctuations in L-mode is shot #35646 (Fig. 7).

From t~5 s, T_e fluctuations show peaks near 20 and 40 kHz, while magnetic spectrum exhibits a ~20 kHz line. The frequency increases across the L–H transition and seems to n_e , T_e . The ~20 kHz feature is consistent with a BAE frequency: $f_{BAE} = \frac{v_{Ti}}{2\pi R} \sqrt{\frac{7}{4}} (1 + \tau_e)$, $v_{Ti} = \sqrt{\frac{2T_i}{m_i}}$ which, for $B_T = 1.9T$, $n_e \approx 3.2 \times 10^9 m^{-3}$, $T_i \sim 300 \text{eV}$ and $R \approx 1.8 \, m$, and $\tau_e = \frac{Te}{Ti} \sim 1$, gives $f_{BAE} \sim 25$ kHz. The ~40 kHz component in T_e may represent the second harmonic, a nearby branch, or diagnostic aliasing. The absence of a clear 40 kHz line in magnetic fluctuations, despite its presence in Te fluctuation, can

be due to frequency-dependent magnetic shielding by conducting structures (skin-depth/eddy-current attenuation).

4.2 Er shear

A strong toroidal rotation V_T driven by the NBI heating dominates the total Er shear,

$$E_r = \frac{1}{Zen} \nabla P - v_\theta B_T + V_T B_\theta \tag{2}$$

particularly, in plasma core. As density increases, we observe a systematic decrease in V_T . The left and middle panels of Fig 8 compare the toroidal velocity profile at low ($n_e = 1.5 \times 10^{19} \text{ m}^{-3}$, 35365) and high density ($n_e = 3.57 \times 10^{19} \text{ m}^{-3}$, 35367). At low density (left), the plasma develops a steeper toroidal velocity $V_T(r)$ profile with higher pedestal-top velocity and higher core toroidal velocity than at high density. The right panel of Fig. 8 compares Er profiles in the L-mode (dashed) and H-mode (solid) at four densities. In all cases, Er becomes negative and develops a steep edge gradient after the L-H transition. In H-mode the lowest-density plasma exhibits the steepest edge gradient and deepest negative Er well; the highest-density case shows the weakest well, with the $n_e = 2.57 \times 10^{19} \text{ m}^{-3}$ and $3.2 \times 10^{19} \text{ m}^{-3}$ cases in between.

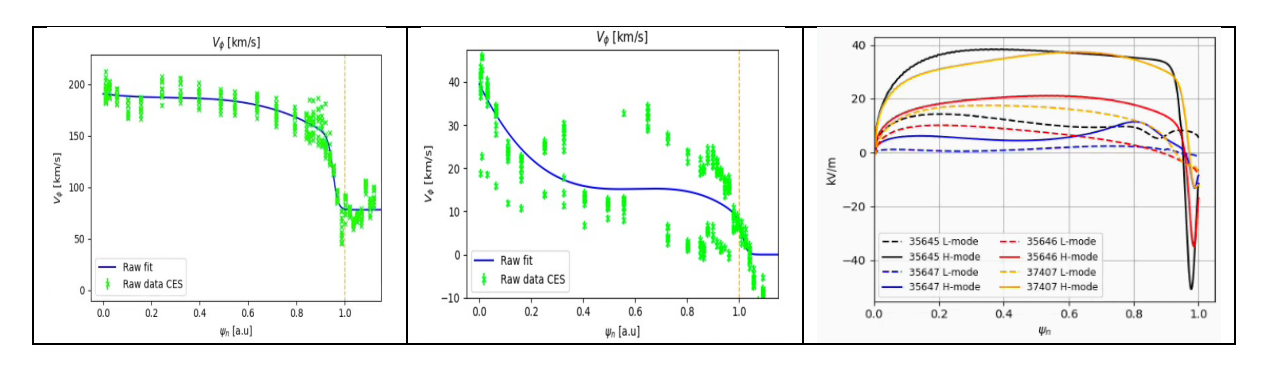


Fig. 8 V_T profiles for 35645 (left) and 35647 (middle); Er profiles for different densities in LSN (right).

5. ERMP EFFECTS

5.1 L-H transition avoidance

We compare a pre-emptive ERMP discharge (#37404) with a conventional ERMP discharge (#35641), in which ERMPs are applied in L-mode and H-mode, respectively. In the conventional case (#35641), ERMPs were applied for 2 s in H-mode (t=10–12 s). Since #35641 entered H-mode at t=5.23 s, the same ERMP settings were applied pre-emptively in #37404 for 1 s during L-mode (t=5–6 s).

Figure 9 compares time traces of key plasma parameters for the conventional ERMP discharge #35641 (black) and the pre-emptive ERMP discharge #37404 (red). The two shots used identical NBI power and exhibited similar parameters up to t=5 s, when ERMPs were switched on in #37404. The ERMPs prevented #37404 from accessing H-mode, whereas the ERMP-free #35641 underwent the L-H transition at t=5.23 s. Shortly after ERMPs were switched off at t=6 s, #37404 transitioned to H-mode at t=6.17 s, followed by an H-L back-transition and a second L-H transition before the discharge was terminated by the onset of large ELMs.

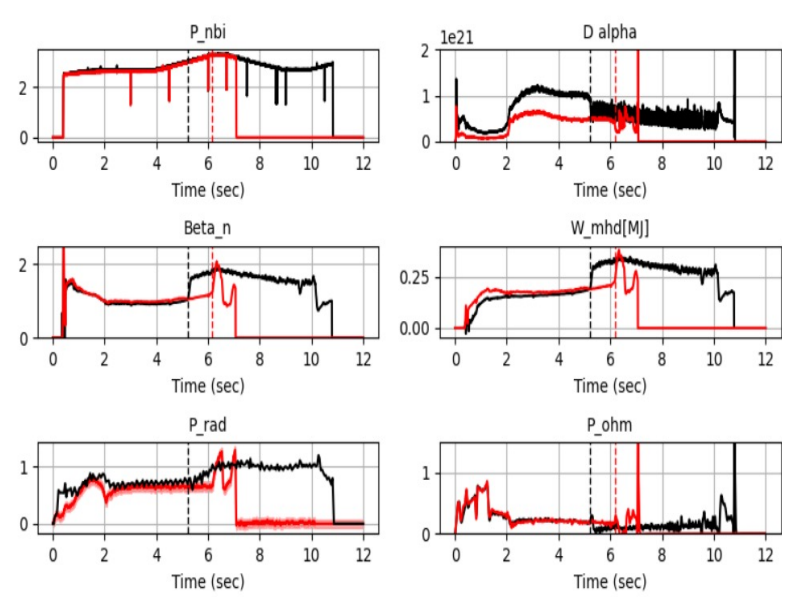


Fig 9. Time-traces of plasma parameters for the conventional ERMP #35641 (black) and pre-emptive ERMP #37404 (red) discharges. L-H transition time is t=5.23 for #35641 and t=7.67 for #37404.

In contrast, the conventional discharge #35641 sustained H-mode for over 5 s and reverted to L-mode shortly after ERMPs were switched on at t=10 s. By comparison, the pre-emptive ERMP case produced a more unstable H-mode of shorter duration, with larger ELMs terminating the plasma after the second L–H transition. Furthermore, as shown in the top panel of Fig. 10, spectra of magnetic and electron-temperature fluctuations in #35641 display coherent modes during t=5.27–5.33 s in H-mode; no such modes are observed in #37404 in the bottom of Fig 10, indicating that ERMPs suppress these coherent features. We note that the coherent modes, when present, appear between ELM bursts.

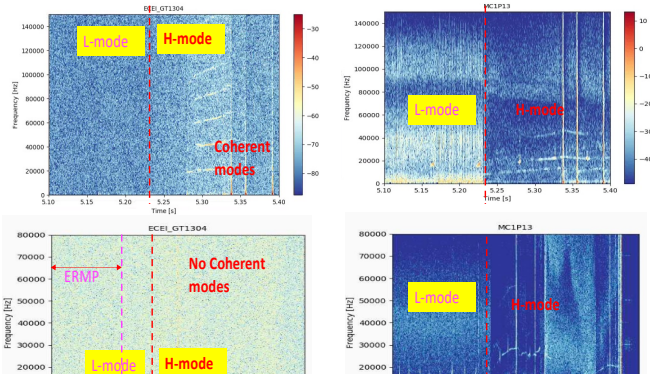


Fig 10. Spectra of Te (left) and magnetic fluctuations (right). Top and bottom are for conventional ERMP #35641 (black) and preemptive ERMP #37404 (red) discharges, respectively.

These results suggest that although the preemptive ERMP shot #37404 had no ERMPs active at the moment of its L−H transition (t≈6.1−6.2 s), it nonetheless entered a different H-mode state than the conventional case #35641. In other words, applying ERMPs at t=5−6 s imprints a history dependence (hysteresis) on the subsequent H-mode.

Nevertheless, the peak plasma energy W_{mhd} and density are higher in the pre-emptive ERMP case, indicating high-performance potential [12] even if only briefly. However, this state is inherently short-lived and more unstable, with an early termination of the discharge. Achieving a

sustained high-performance H-mode via pre-emptive ERMPs will therefore require a careful optimization of the ERMP timing, amplitude, and spectral content.

5.2 ELM suppression

In addition to H-mode avoidance and H-L transition trigger reported above, ERMPs are shown to suppress ELMs transiently in plasma discharge #35640, shown in Figure 11. Specifically, after the switch-on of ERMPs at t=10 secs, D α shows the suppression of ELMs around t=10.5, 10.6 secs for short times. Notably, ERMPs alter the magnetic spectrograms shown in the right panel of Figure 11. Specifically, at t=10.1 secs (when the ERMP is the maximum), MP1P03 (outboard probe) shows the change in the low-frequency oscillations, magnetic fluctuations around 24 kHz and 12 kHz merging into one frequency \sim 16 kHz, becoming more similar to what is seen in MP1P13 (inboard probe). This can imply a synchronisation of edge-core dynamics through ERMPs. Furthermore, magnetic fluctuations in MP1P03 become broader and develop coherent modes at t=10.5, 10.6 secs.

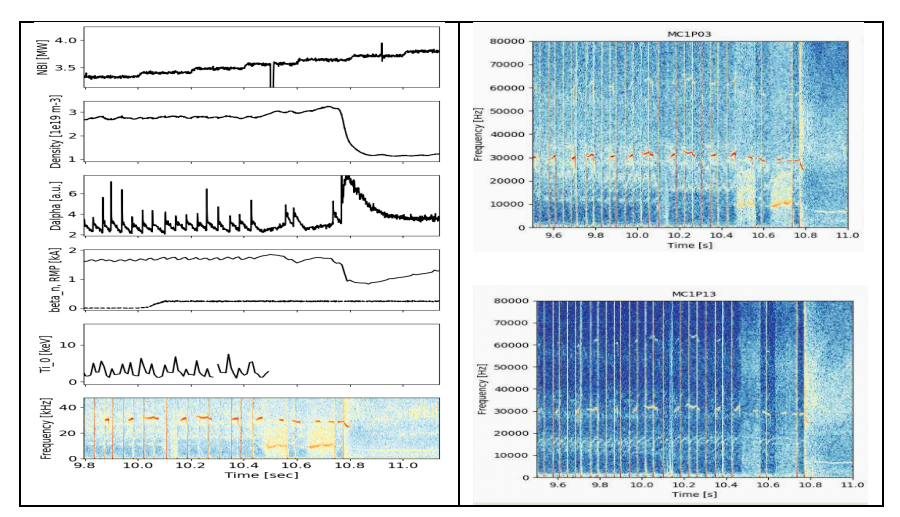


Fig 11. #35640 with ERMPs on t=[10,12] secs. (Left) The time-evolution of the key plasma parameters; (right) Magneto spectra of the outboard MP1P03 (top) and inboard MP1013 (bottom) Mirnov channels.

6. CONCLUSION

We demonstrated the importance of hidden variables and magnetic fluctuations in understanding the L-H/H-L transition. In particular,

- Hidden-variables: Ramping history (and impurities) affects L-H/H-L access. Different power-ramp scenarios introduce significant scatter in the L-H power threshold, consistent with theory.
- Configuration and density: USN requires more power than LSN (often by a factor \geq 2). The threshold shows a rollover with a minimum near $n_e \approx 2.5 \times 10^{19} \text{ m}^{-3}$.
- Ubiquitous magnetic fluctuations, role varies with density and geometry:
 - Low-density LSN: broadband magnetic and density fluctuations are suppressed at L-H; quasicoherent lines at ~10-20 kHz persist and shift upward with heating while broadband electron temperature fluctuations can remain.
 - Higher-density and/or USN: magnetic fluctuations correlate more strongly with density fluctuations than with electron temperature fluctuations, consistent with pressure-coupled EM modes dominating.
- ERMP effects are multi-faceted: they can delay or avoid L-H, trigger H-L, suppress ELMs, restructure spectra (e.g., frequency merging and probe-to-probe synchronization), and imprint hysteresis. Pre-emptive ERMPs can yield higher peak W_{mhd} and n_e but a short-lived, more unstable H-mode with larger ELMs.
- Rotation/momentum: in H-mode with strong multi-channel fluctuations, toroidal-rotation shear decreases at plasma edge, indicating enhanced momentum transport and/or altered net external torque.

Our results highlight the importance of hidden variables, optimizing ramping strategy, tailoring ERMP timing/amplitude/spectrum, and controlling various EM modes across density and magnetic configuration for high-performance H-mode.

ACKNOWLEDGEMENTS

This research is supported by Brain Pool Program funded by the Ministry of Science and ICT through the National Research Foundation of Korea (RS- 2023-00284119). EK thanks Xavier Garbet and Yasmin Andrew for helpful discussions.

REFERENCES

- [1] Martin, Y.R. J. Phys.: Conf. Ser. 123 (2008) 012033
- [2] Howlett, L. Nucl. Fusion 63 (2023) 052001
- [3] Aston-Key, T... Kim, E. et al., Plasma Phys. Control. Fusion 67 (2025) 025027
- [4] Kim, E. et al., Plasma Phys. Control. Fusion 67 (2025) 025025
- [5] Solano, E.R. et al., Nucl. Fusion 57 (2017) 022021
- [6] Yang, S.M. et al, Nature Communications 15 (2024) 1275
- [7] Drake, J.F. et al., Phys. Rev. Lett. 44 (1980) 994
- [8] Heidbrink W.W., Phys. Plasmas 15 (2008), 055501
- [9] Chen, L. and Zonca, F. Mod. Phys. 88 (2016), 015008
- [10] Kotschenreuther, M. et al, Nucl. Fusion 59 (2019) 096001
- [11] Appert, K., Plasma Physics 24 (1980), 1147
- [12] Kim, M. et al., Nucl. Fusion 63 (2023) 08603